Food Chemistry 463 (2025) 141341

Contents lists available at ScienceDirect

Food Chemistry

journal homepage: www.elsevier.com/locate/foodchem

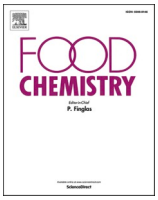

New application of a dye-decolorizing peroxidase immobilized on magnetic nanoparticles for efficient simultaneous degradation of two mycotoxins

Xinling Du [a,1], Mumin Zheng [b,1], Han Zhang [a], Yangyu Qiu [a], Fuchun Ji [a], Zishen Nie [a], Huidong Xu [a], Xiaoxuan Li [a], Shijia Wu [a], Zhouping Wang [a], Fuguo Xing [b,*], Yu Xia [a,*]

[a] State Key Laboratory of Food Science and Technology, School of Food Science and Technology, Jiangnan University, Wuxi 214122, China
[b] Institute of Food Science and Technology, Chinese Academy of Agricultural Sciences, Beijing 100193, China

ARTICLE INFO

Keywords:
Dye-decolorizing peroxidase
Magnetic nanoparticle
Enzyme immobilization
Mycotoxin
Degradation

ABSTRACT

Nowadays the enzymatic approaches are the most promising strategies for mycotoxins detoxification in food stuffs. Herein, the dye-decolorizing peroxidase RhDypB from *Rhodococcus jostii* was studied for its ability to degrade two mycotoxins in both free and the immobilized enzyme forms. This enzyme was recombinantly expressed and purified, while Fe_3O_4 nanoparticles were prepared and modified with chitosan as the immobilization carrier. The immobilized enzyme Fe_3O_4@CS@RhDypB demonstrated degradation rate of 85.61 % toward aflatoxin B_1, while it was firstly found to be able to degrade zearalenone with the rate of 86.52 %, at pH 4.0 on 30 °C. The degradation products were identified as aflatoxin Q_1 and 15-OH-ZEN respectively. After 5 cycles of reuse, Fe_3O_4@CS@RhDypB still exhibited degradation rates of 38.50 % and 49.76 % toward the mycotoxins, indicating its high reusability. Moreover, Fe_3O_4@CS@RhDypB exhibited excellent stability after 10 days of storage. This work identified potential applications of nanoparticle-immobilized enzyme for biodegradation of mycotoxins in food industry.

1. Introduction

Mycotoxins, which occur in foodstuffs such as peanuts, corn, and other grains, are related to human health and have attracted the consumer's attention. Currently, more than 300 kinds of mycotoxins have been detected and characterized, however, only a few mycotoxins dominate in contaminated food or feed. Among them, aflatoxins (AFs), and zearalenone (ZEN) as major fungal toxins, have caused serious economic loss worldwide and exerted adverse effects on humans and animals (Alshannaq & Yu, 2017; Escrivá, Font, Manyes, & Berrada, 2017). AFs, as a group of secondary metabolites produced by the fungus genus *Aspergillus* (such as *A. flavus*, *A. parasiticus*, and *A. nomius*), are associated with liver carcinogenesis, neurotoxicity, and growth retardation. Aflatoxin B_1 (AFB_1) is the most prominent and toxic member of this group (Engin & Engin, 2019; Pickova, Ostry, Toman, & Malir, 2021). ZEN, biosynthesized by several *Fusarium* species, possesses a high binding affinity to estrogen receptors, leading to reproductive diseases involving infertility, ovarian disease, reduced sperm counts, pseudopregnancy, and endometrial disease (Wang et al., 2024; Zhou et al., 2024). Consequently, many countries have established maximum limits for multiple mycotoxins in food and feed due to their risk to humans and animals (Sobral, Faria, Cunha, & Ferreira, 2018).

Given that the widespread mycotoxins have been a vital aspect of the safety and quality of food, it is urgent to explore an effective method for mycotoxin detoxification. So far, there are common ways for mycotoxin degradation that can be classified into physical, chemical, and biological methods (Adebo et al., 2020; Xia et al., 2022). Among them, the biological methods, which utilize alive microorganisms, expressed enzymes, and microbial metabolites, have been gradually considered the most sustainable and environmentally friendly approach to control mycotoxin levels (Shi et al., 2023; Wang, Chen, Jiang, & Huang, 2022).

Dye-decolorizing peroxidases (DyPs) are a novel family of peroxidases with heme as a cofactor. It has been reported that DyPs exhibit activity toward a wide range of substrates, involving lignin-derived phenolic and non-phenolic compounds (Mangini et al., 2024). DyPs exhibit unique catalytic mechanisms and superior properties, including a high redox potential, which enable them to act on a broad spectrum of substrates and reactions. These characteristics render DyPs an optimal

* Corresponding authors.
E-mail addresses: xingfuguo@caas.cn (F. Xing), yuxia@jiangnan.edu.cn (Y. Xia).
[1] **These authors contributed equally to this work.**

https://doi.org/10.1016/j.foodchem.2024.141341
Received 16 July 2024; Received in revised form 6 September 2024; Accepted 15 September 2024
Available online 17 September 2024

choice for mycotoxin degradation. Currently, several earlier investigators have described that DyPs had good detoxification capacity for part of mycotoxins due to their unique structural and catalytic properties (Qin et al., 2021). Compared with other mycotoxin degradation enzymes, DyPs do not require additional mediators. Noteworthy, RhDypB, a DyP from *Rhodococcus jostii*, has shown an impressive rate of mycotoxin degradation, highlighting its ability to combine various dye-decolorizing and oxidative activities within a single enzyme (Vignali, Tonin, Pollegioni, & Rosini, 2018). However, the practical application of DyPs is hindered by their limited stability, non-reusability, and challenges in separating them from complex reaction matrices.

Fortunately, the immobilization enzyme represents a promising way to address the above problem. Recently, magnetic nanomaterials have gained increasing attention due to their large surface, easy separation by the magnet, and high stability in a broad range of temperatures (Li et al., 2018). Hence, magnetic nanomaterials are attractive materials that serve as the carrier for enzyme immobilization. Additionally, biosensors and catalysts based on magnetic nanomaterials have also been developed and exhibit potential applications in the food industry (Vaghari et al., 2016). However, the aggregation tendency and lack of functional groups in Fe_3O_4 nanoparticles pose a significant challenge that needs to be efficiently addressed. Chitosan, as deacetylated chitin, is abundantly available in nature and has been employed as a favorable functional component in many fields due to its low toxicity and good biocompatibility (Li et al., 2018). Besides, the efficiency for enzyme immobilization of the magnetic nanomaterials is improved by modifying with chitosan.

In this work, the recombinant dye-decolorizing peroxidase RhDypB from *Rhodococcus jostii* was expressed in *Escherichia coli*. The magnetic nanoparticles modified with chitosan (Fe_3O_4@CS) were subsequently prepared for immobilization of RhDypB, and the properties of immobilized RhDypB (Fe_3O_4@CS@RhDypB) were characterized. Meanwhile, we used Fe_3O_4@CS@RhDypB for mycotoxin degradation. It was found that the hydroxylation of AFB_1 and ZEN by Fe_3O_4@CS@RhDypB resulted in the degradation products of AFQ_1 and 15-OH-ZEN. In addition, we investigated the reusability and storage stability of Fe_3O_4@CS@RhDypB for mycotoxin degradation. All the results indicated that Fe_3O_4@CS@RhDypB had excellent enzymatic activity, high reusability and good storage stability, and it has potential applications in mycotoxin detoxification.

2. Materials and methods

2.1. Materials and agents

The chemicals $FeSO_4{\cdot}7H_2O$, chitosan, NaOH, and glutaraldehyde were purchased from Sinopharm Chemical Reagent Co., Ltd. (Shanghai, China). The mycotoxins AFB_1 and ZEN were purchased from Pribolab (Shandong, China). In this work, the stock solution of the mycotoxins AFB_1 and ZEN was separately prepared at a final concentration of 1.0 mg/mL using acetonitrile as the solvent. All the standards were stored in darkness at −20 °C. The chemicals methanol, acetonitrile, hemin, substrates 2,2-Azino-bis (3-ethylbenzothiazoline-6-sulfonic acid) (ABTS), isopropyl β-D-1-thiogalactopyranoside (IPTG), and ethanol (EA) were purchased from Sangon Biotech Co., Ltd. (Shanghai, China). All restriction enzymes were purchased from Thermo Fisher Scientific (Shanghai, China). The gene of RhDypB (GenBank Accession No. MH292860), which fused with a 6 × his tag at C-terminus, was synthesized and subcloned into the pET28a between *Nco*I and *Xho*I restriction sites by GenScript Biotech Co., Ltd. (Nanjing, China).

2.2. Expression, and characterization of dye-decolorizing peroxidase RhDypB

The gene of RhDypB was cloned into the pET28a vector and transformed into *E. coli* BL21(DE3) host, as depicted in Fig. S1. The recombinant strain *E. coli* BL21(DE3, pET28a-RhDypB) was utilized for RhDypB expression. The recombinant strain was cultured in liquid LB medium (10 g/L tryptone, 5 g/L yeast extract, 10 g/L NaCl) containing 50 μg/mL kanamycin overnight at 37 °C. Subsequently, the cells were grown in TB medium (24 g/L yeast extract, 12 g/L bacto-tryptone, 8 mL/L glycerol, 9.4 g/L K_2HPO_4, 2.2 g/L KH_2PO_4). The inducer IPTG at a final concentration of 1.0 mmol/L and hemin at a final concentration of 0.25 g/L were added to the medium when the OD_{600} reached 1.0 and the recombinant strain was induced at 18 °C with a slow induction speed for 20 h. RhDypB, a glycoprotein that requires hemin as a cofactor, benefits from a slow induction speed to promote hemin incorporation (Sugano, Muramatsu, Ichiyanagi, Sato, & Shoda, 2007; Vignali et al., 2018). Finally, the cells were harvested by centrifugation at 8000 rpm for 10 min at 4 °C. Then the cells were resuspended in Tris-HCl buffer (50 mmol/L, pH 7.4), and ultrasonically disrupted on ice for 15 min (ultrasonic, 2 s; pause, 1 s). The lysates were centrifuged to remove cell debris at 8000 rpm for 15 min at 4 °C. The enzyme was purified via the HisTrap HP Ni-NTA column (Cytiva, USA). Then the purified RhDypB was analyzed by sodium dodecyl sulfate-polyacrylamide gel electrophoresis (SDS-PAGE).

Then the purified enzyme was subject to UV–visible spectroscopy analysis. A volume of 200 μL of the purified enzyme was used to measure the absorbance within the range of 280–700 nm. The Reinheitzahl value (Rz value) was calculated by determining the ratio of absorbance at 420 nm to the absorbance at 280 nm.

The kinetic parameters of the enzyme were determined by monitoring the oxidation rate of the ABTS at various concentrations. The reaction system consisted of 50 mmol/L malonic acid buffer (pH 4.0), 10 mmol/L $MnCl_2$, 0.1 mmol/L H_2O_2, and 5 μL free RhDypB. Subsequently, the substrate, ABTS, was added at concentrations ranging from 0.1 mmol/L to 10 mmol/L, and the rate of enzymatic reaction was measured. Finally, the values of K_m and k_{cat} were calculated.

2.3. Preparation of the immobilized enzyme Fe_3O_4@CS@RhDypB

2.3.1. Preparation of Fe_3O_4 nanoparticles

The preparation scheme was depicted in Fig. 1. The Fe_3O_4 was synthetized by using the chemical method. Specifically, 1.39 g of $FeSO_4{\cdot}7H_2O$ was dissolved in 100 mL water, and the pH was adjusted to 10.0 using NaOH. Then the solution was continuously stirred at 25 °C for 15 min. After stopping stirring, the resulting products were magnetically separated and subsequently washed three times with ethanol and ultrapure water, respectively. Then, the Fe_3O_4 nanoparticles were dried under vacuum at 40 °C for 12 h.

2.3.2. Preparation of Fe_3O_4@CS nanoparticles

For the preparation of Fe_3O_4@CS, 0.1 g of Fe_3O_4 was diffused into 100 mL chitosan solution (4.0 mg/mL) that was dissolved with 1 % acetic acid. To act as a metal chelator, 50 mL of sodium tripolyphosphate solution (0.8 mg/mL) was added, and the mixture was subjected to ultrasonic treatment at room temperature for 40 min. Subsequently, the Fe_3O_4@CS nanoparticles were separated by an external magnetic field and washed several times with ethanol. Finally, the Fe_3O_4@CS composite nanoparticles were dried under vacuum at 40 °C for 6 h.

2.3.3. Immobilization of RhDypB onto Fe_3O_4@CS carrier

For the preparation of Fe_3O_4@CS@RhDypB, 0.05 g of Fe_3O_4@CS was suspended in 1 mL 1 % glutaraldehyde solution at 25 °C for 3 h. Then, the activated Fe_3O_4@CS nanoparticles were separated by the magnet and washed three times with sodium acetate buffer (50 mmol/L, pH 4.0). The Fe_3O_4@CS carrier was immersed in purified RhDypB for immobilization at room temperature for 6 h. After immobilization, the Fe_3O_4@CS@RhDypB was magnetically separated and washed several times with sodium acetate buffer. For storage and future use, the Fe_3O_4@CS@RhDypB was stored at the buffer at 4 °C. The protein concentration was calculated by the BCA protein quantitative assay kit

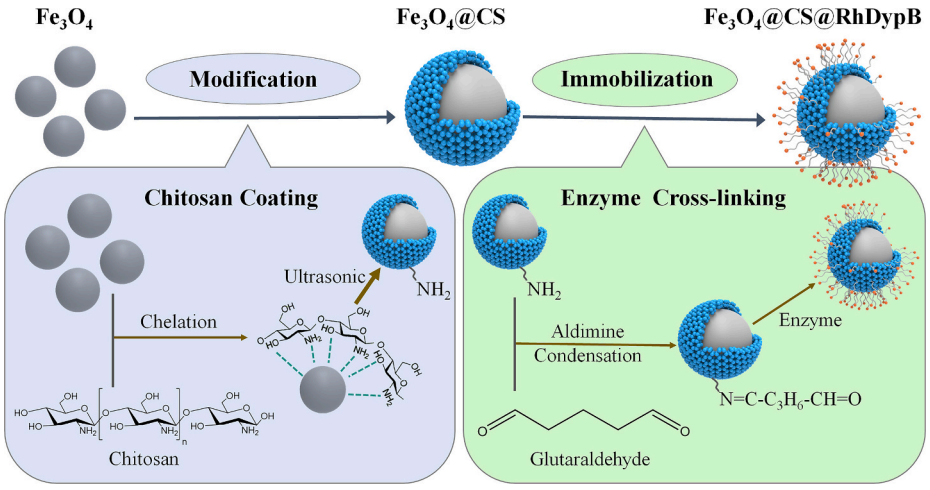

Fig. 1. The scheme for preparation of chitosan-modified magnetic nanoparticles (Fe_3O_4@CS) and immobilization of RhDypB (Fe_3O_4@CS@RhDypB).

(Sangon Biotech, Shanghai, China) to determine the protein loading capacity.

The protein load calculation formula was as follows:

$$\text{Protein loading capacity (mg/g)} = \frac{(C_0 - C)\,V}{m} \quad (1)$$

C_0 (mg/mL) represents the initial concentration of free enzyme, C (mg/mL) represents the residual concentration of free enzyme, V (mL) represents the volume of the enzyme solution, and m (g) represents to the mass of the carrier.

The enzymatic activity recovery was as follows:

$$\text{Enzymatic activity recovery (\%)} = \frac{X_1}{X_2} \times 100 \quad (2)$$

X_1 represents the enzymatic activity of the Fe_3O_4@CS@RhDypB, X_2 represents the enzymatic activity of the free enzyme.

2.4. Characterization of Fe_3O_4@CS@RhDypB

The particle size and dispersibility of composite nanoparticles were observed by scanning electron microscopy (SEM) (S4800, Hitachi, Japan) operated at 10 kV. Fourier transform infrared spectroscopy (FT-IR) spectra were characterized by KBr pellets on an FT-IR spectrophotometer (Varian 3100, Varian, USA). The wavenumber was 4000 cm^{-1} to 400 cm^{-1}. X-Ray Diffractometer (XRD) pattern was obtained on a Rigaku-12KW X-ray diffractometer. The scanning range was 20°-80°, the scanning rate was 8°/min, and the Cu target Kα ($\lambda = 0.15406$ nm) was used as the X-ray source. The magnetic property was detected by a vibrating sample magnetometer (VSM, Lakeshore). The measured magnetic field range was −2000 to 2000 Oe, and the temperature of the measurements was room temperature.

2.5. Optimization of preparation of Fe_3O_4@CS@RhDypB

To obtain the optimal preparation conditions of Fe_3O_4@CS@RhDypB, the effects of the amount of enzyme, pH, temperature, cross-linking time, and the concentration of glutaraldehyde were investigated. Firstly, 0.05 g Fe_3O_4@CS was suspended in 1 mL 0.5 %–3.0 % glutaraldehyde solution. Subsequently, the Fe_3O_4@CS nanoparticles were immersed into purified RhDypB with enzyme amounts ranging from 0.5 U to 5 U, at various pH values (2.0–8.0) and temperatures (25–75 °C) for durations of 20–120 min. The optimal conditions were characterized by the enzymatic activity recovery and the protein loading capacity as described above.

2.6. Study of enzymatic activity between free RhDypB and Fe_3O_4@CS@RhDypB

Compared with pyrogallol, and Reactive Blue 4, RhDypB showed the greatest apparent specificity for ABTS (Roberts et al., 2011). So the enzyme activities were characterized by monitoring the oxidation of ABTS, which served as the substrate (Loi et al., 2020). The total reaction volume contained 50 mmol/L malonate buffer (pH 4.0), 10 mmol/L $MnCl_2$, 0.1 mmol/L H_2O_2, 1 mmol/L ABTS, 5 μL free RhDypB or 20 μL Fe_3O_4@CS@RhDypB suspension. The change of absorbance at the wavelength of 420 nm was recorded by a microplate reader. Enzymatic activity was quantified as one unit (1 U), defined as the amount of enzyme that oxidizes 1 mmol/L of ABTS per minute at 30 °C.

To investigate the effect of pH on both free RhDypB and Fe_3O_4@CS@RhDypB, enzymatic activities were assayed at 30 °C with a pH range of 2.0 to 8.0. Similarly, to investigate the effects of temperatures on both free RhDypB and Fe_3O_4@CS@RhDypB, enzymatic activities were assayed at pH 4.0 across temperatures ranging from 15 °C to 85 °C. The highest enzymatic activity was set as 100 %.

For exploring the storage stability, RhDypB, both in its free and immobilized forms, was stored in 50 mmol/L malonate buffer (pH 4.0) at 4 °C. The enzyme activity of both was measured every three days (72 h). To assess reusability, the Fe_3O_4@CS@RhDypB was magnetically separated and washed with ultrapure water after each use. The recovered Fe_3O_4@CS@RhDypB was promptly introduced into the new reaction system to assess its enzymatic activity. Each measurement of the enzymatic activity of Fe_3O_4@CS@RhDypB was considered as one instance of usage. The initial enzymatic activity was set as 100 %.

2.7. Investigation of mycotoxin degradation by Fe_3O_4@CS@RhDypB

For the investigation of mycotoxin degradation by Fe_3O_4@CS@RhDypB, two specific mycotoxins, AFB_1 and ZEN, were employed. The mycotoxin degradation tests were carried out in 50 mmol/L malonate buffer (pH 4.0) containing 10 mmol/L $MnCl_2$, 0.1 mmol/L H_2O_2, 1.0 μg/mL AFB_1 or ZEN, and 50 μL Fe_3O_4@CS@RhDypB suspension (Loi et al., 2020). The resulting mixture was incubated at 30 °C for a duration of 24 h. After incubation, the Fe_3O_4@CS@RhDypB was magnetically separated, and the supernatants were filtered through a 0.22 μm filter for mycotoxin detection. The detection of AFB_1 and ZEN performed by UPLC-MS referred to the previous study (Xia et al., 2022). The detection instrument was the UPLC-TQD from Waters Corporation (Milford, MA, United States). Detection of AFB_1 used electrospray ionization in positive ion mode whereas detection of ZEN used electrospray ionization in negative ion mode. The chromatographic column was the ACQUITY

UPLC BEH C18 column (2.1 × 50 mm, 1.7 μm particle size) from Waters Corporation (Milford, MA, United States). The AFB_1 and ZEN standard samples were prepared in acetonitrile with the concentration gradients (0.1, 0.2, 0.5, 1.0, 2.0, and 5.0 μg/mL) to establish the standard curve for AFB_1 and ZEN concentration calculation. Control samples were prepared by substituting the Fe_3O_4@CS@RhDypB suspension with equal amounts of Fe_3O_4 and Fe_3O_4@CS suspension. Each reaction was repeated three times.

The reusability of Fe_3O_4@CS@RhDypB was evaluated in the aforementioned reaction system. Each 24 h degradation reaction using Fe_3O_4@CS@RhDypB was considered as one instance of usage. After the completion of the reaction, the Fe_3O_4@CS@RhDypB was separated using the magnet and subsequently washed with ultrapure water several times to remove the residual mixture. The Fe_3O_4@CS@RhDypB was then immediately added to the new reaction mixture, and the degradation tests were repeated.

For exploring the storage stability, Fe_3O_4@CS@RhDypB was stored in 50 mmol/L malonate buffer (pH 4.0) at 4 °C. A certain amount of Fe_3O_4@CS@RhDypB suspension was taken every day for mycotoxin degradation analysis.

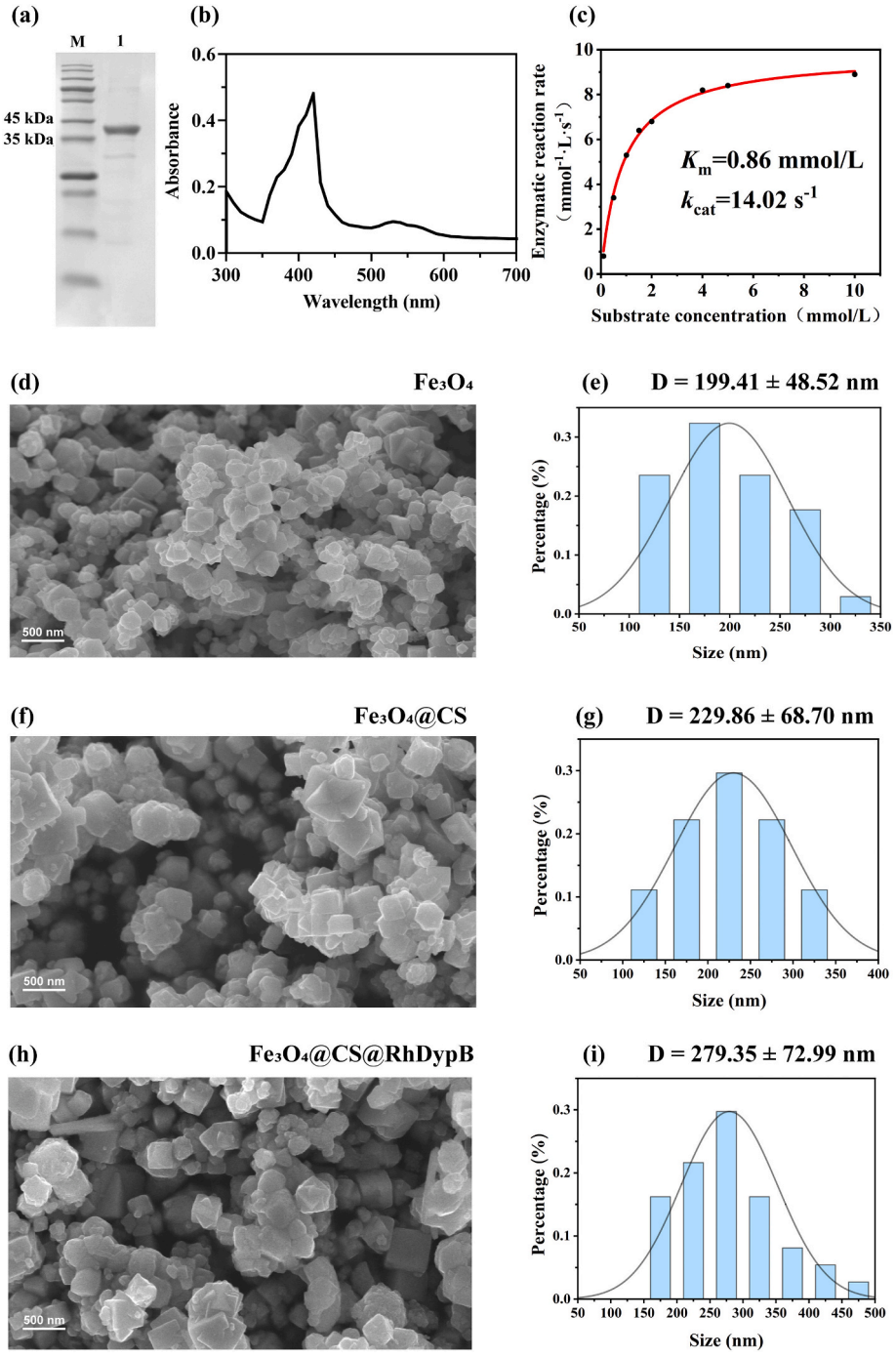

Fig. 2. Analysis of RhDypB and SEM images and DLS size distributions of the immobilized enzyme Fe_3O_4@CS@RhDypB. (a) SDS-PAGE analysis of purified RhDypB. Lane M, protein marker; lane 1, purified RhDypB. (b) UV–visible absorption spectrum of purified RhDypB. (c) Enzyme reaction kinetics analysis of RhDypB with ABTS as substrate. (d) SEM images of Fe_3O_4. (e) DLS size distributions of Fe_3O_4. (f) SEM images of Fe_3O_4@CS. (g) DLS size distributions of Fe_3O_4@CS. (h) SEM images of Fe_3O_4@CS@RhDypB. (i) DLS size distributions of Fe_3O_4@CS@RhDypB.

2.8. Identification of mycotoxin degradation products

The degradation products of AFB_1 and ZEN were subjected to UPLC-MS analysis. The liquid chromatography detector was WATERS ACQUITY PDA from Waters Corporation (Milford, MA, United States), and the detection wavelength was 200-400 nm. The liquid chromatographic separation was executed on an ACQUITY UPLC BEH C18 column (2.1 mm × 150 mm, 1.7 μm particle size) from Waters Corporation (Milford, MA, United States) at 45 °C. The mobile phase A was acetonitrile and the mobile phase B was 0.1 % formic acid. The injection volume was 5 μL and the flow rate was set at 0.3 mL/min. The ion source temperature was maintained at 100 °C, and the desolvation gas temperature was set to 400 °C. The mass parameters were as follows: capillary voltage of 3.5 k*V*, capillary temperature of 400 °C, cone voltage of 30 V, collision energy of 20 eV, and a scan range of 20–2000 *m/z*.

3. Results and discussion

3.1. Expression, purification, and characterization of RhDypB

The enzyme RhDypB was expressed and purified according to the method in Section 2.2, and it was analyzed by SDS-PAGE. A single band with a molecular mass of about 40 kDa was observed, corresponding to the theoretical molecular mass of RhDypB (Fig. 2a).

Upon closer examination of Fig. 2a, an additional band was identified, which may have implications for the purity of the protein preparation. In our previous experiments, the recombinant strain *E. coli* BL21 (DE3, pET28a) was expressed with induction, and the subsequent analysis using SDS-PAGE indicated that the cell-free extract of this strain exhibited band similar to the unexpected protein showed in Fig. 2a. However, no obvious degradation effect of mycotoxins was observed using the unexpected protein samples. Therefore, it can be concluded that the presence of this additional band did not substantially impact the validity of our findings.

In addition, the RhDypB showed the typical features of hemin-containing enzymes with a Soret peak of about 420 nm, as indicated in Fig. 2b (Colpa, Fraaije, & van Bloois, 2014). The presence of this peak implied that the hemin had indeed participated during the protein folding process. The Rz value (Reinheitzahl value, defined by the rate between the Soret absorbance at 420 nm and the absorbance at 280 nm) of the purified RhDypB was 2.4, which was similar to the previous study (Vignali et al., 2018).

The catalytic efficiency of RhDypB on substrate ABTS can be represented by k_{cat}/K_m. A larger k_{cat}/K_m value indicates higher catalytic efficiency of RhDypB on substrate ABTS. To investigate the impact of varying concentrations of ABTS on the reaction rate of recombinant enzyme RhDypB, the enzymatic reaction rate of RhDypB was determined under different ABTS concentrations at pH 4.0 and 30 °C. RhDypB had a K_m value of 0.86 mmol/L and a k_{cat} value of 14.02 s^{-1}, resulting in a k_{cat}/K_m value of 16.30 $mmol^{-1}{\cdot}L{\cdot}s^{-1}$ (Fig. 2c). The enzyme kinetic parameters of dye-decolorizing peroxidase (DyPs) from various microbial sources were presented (Table. 1). The results indicated that RhDypB had high catalytic efficiency and capacity, making it suitable for subsequent experiments.

3.2. Immobilization of RhDypB onto magnetic chitosan and characterization

3.2.1. SEM analysis

The morphologies and particle sizes of Fe_3O_4, Fe_3O_4@CS, and Fe_3O_4@CS@RhDypB were characterized by SEM (Fig. 2d, f, h). The results revealed that all samples were presented as cubes and had good dispersity. The particle sizes of these samples were further measured, which were approximately 199.41 ± 48.52, 229.86 ± 68.70, and 279.35 ± 72.99 nm, respectively. It was observed that the sizes of the three materials followed a normal distribution, indicating a relatively uniform particle size distribution (Fig. 2e, g, i). The increase in size for Fe_3O_4@CS and Fe_3O_4@CS@RhDypB compared to Fe_3O_4 may be attributed to the chitosan coating and enzyme immobilization on the Fe_3O_4 surface, confirming the successful preparation of Fe_3O_4@CS, and Fe_3O_4@CS@RhDypB.

3.2.2. FT-IR analysis

The characteristic functional groups of Fe_3O_4, Fe_3O_4@CS, and Fe_3O_4@CS@RhDypB were characterized by FT-IR (Fig. 3a). The typical characteristic absorption peaks of 580 cm^{-1}, and 581 cm^{-1} were relevant to the vibration of Fe—O in Fe_3O_4 (Chen et al., 2018). The absorption peaks at 1624 cm^{-1}, 3444 cm^{-1}, and 3435 cm^{-1} were due to O—H stretching vibrations of water molecules and Fe_3O_4 surface hydroxyl groups or adsorbed water (Farimani, Shahtahmasebi, Rezaee Roknabadi, Ghows and Kazemi, 2013). Meanwhile, the absorption peaks of 1420 cm^{-1} were assigned to N—H bending of chitosan and enzyme molecules, and the absorption peaks at 1050 cm^{-1} and 1097 cm^{-1} were attributed to the C—O stretching vibration (Chen et al., 2018). The weak absorption peaks of N—H and C—O were attributed to the relatively lower quantity of chitosan and enzymes compared to Fe_3O_4 nanoparticles, and this phenomenon was consistent with the previous study (Chen et al., 2018). The above spectral results indicated that chitosan was successfully coated on the surface of Fe_3O_4 nanoparticles and verified the successful preparation of Fe_3O_4@CS@RhDypB.

3.2.3. XRD analysis

The XRD patterns of Fe_3O_4, Fe_3O_4@CS and Fe_3O_4@CS@RhDypB were shown in Fig. 3b. It can be seen that the characteristic peaks at 2θ = 30.06°, 35.4°, 43.04°, 53.4°, 57.2°, and 62.5° were indexed to (220), (311), (400), (422), (511), and (440) crystal planes, respectively. These peaks were consistent with the standard caliper JCPDS 19–0629, confirming the highly cubic inverse spinel structure of the synthesized Fe_3O_4 nanoparticles (Xu, Bi, He, Zhu, & Chen, 2014). The similar characteristic peaks at diffraction patterns of Fe_3O_4@CS and Fe_3O_4@CS@RhDypB indicated that the modification of chitosan and enzyme immobilization did not affect the crystal structure of Fe_3O_4. However, the peak intensities of Fe_3O_4@CS and Fe_3O_4@CS@RhDypB were slightly decreased compared to Fe_3O_4. This phenomenon could be

Table 1
Enzyme kinetic constants of different dye-decolorizing peroxidases.

Enzyme	Microbial source	K_m (mmol/L)	k_{cat} (s^{-1})	k_{cat}/K_m ($mmol^{-1}{\cdot}L{\cdot}s^{-1}$)	substrate	reference
RhDypB	*Rhodococcus jostii* RHA1	0.86	14.02	16.30	ABTS	This text
DtpA	*Streptomyces lividans*	0.73	1.12	1.53	ABTS	(Chaplin, Wilson, & Worrall, 2017)
PputA514_2985	*Pseudomonas putida* A514	0.585	4.846	8.287	ABTS	(Lin, Wang, Cao, & Xu, 2019)
Dyp1B	*Pseudomonas fluorescens* pf-5	1.13	13.5	11.94	ABTS	(Rahmanpour & Bugg, 2015)
PpDyp	*Pseudomonas putida* KT2440	2.5	20	8	ABTS	(Lin et al., 2019)
SaDyP2	*Streptomyces avermitilis*	0.79	1.21	1.71	ABTS	(Sugawara et al., 2017)
PpDyp	*Pseudomonas putida* MET94	1.349	17	12.6	ABTS	(Scocozza et al., 2021)

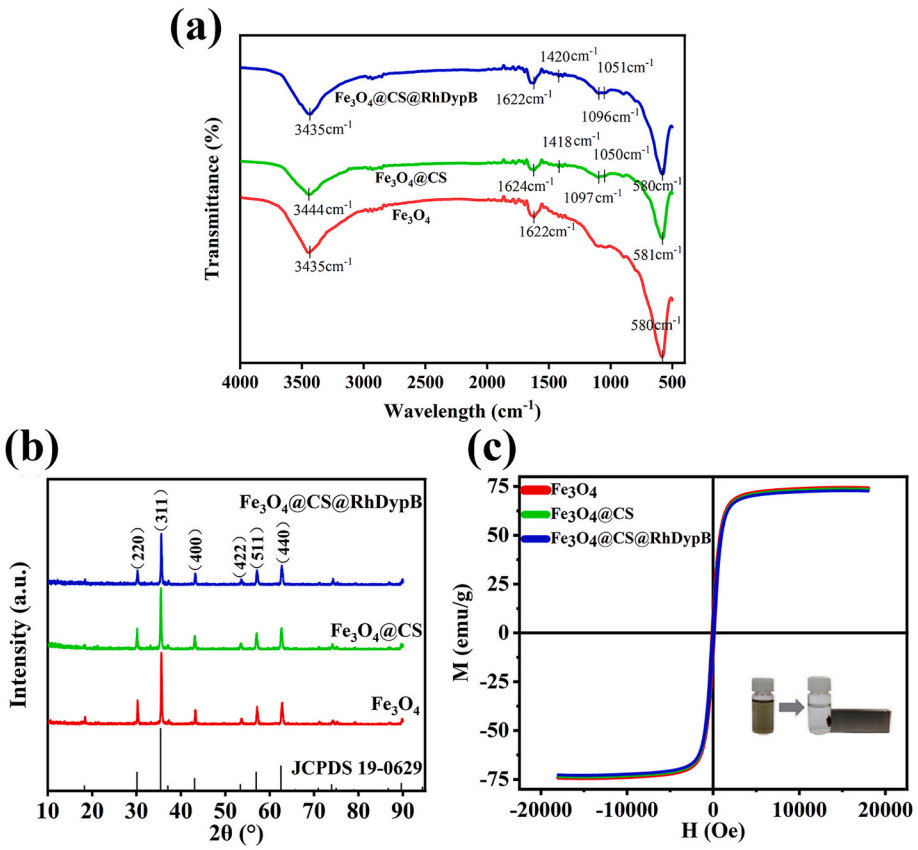

Fig. 3. FT-IR, XRD, and magnetic measurements analysis of Fe_3O_4, Fe_3O_4@CS, and Fe_3O_4@CS@RhDypB. (a) FT-IR analysis results. (b) XRD results. (c) Magnetization curves. Magnetization (M) was expressed in emu/g.

attributed to the coating of chitosan and enzymes leading to a decrease in the degree of crystallization of Fe_3O_4, similar to the previous studies (Xu et al., 2014).

3.2.4. *Magnetic measurements*

The magnetism was tested with VSM (Fig. 3c). The saturation magnetization values for Fe_3O_4, Fe_3O_4@CS, and Fe_3O_4@CS@RhDypB were 74.08, 73.44 and 72.63 emu/g, respectively. A slight decrease in magnetization observed in Fe_3O_4@CS and Fe_3O_4@CS@RhDypB might be due to the existence of chitosan and RhDypB coating on the surface of Fe_3O_4 nanoparticles. It was noted that no significant indication of hysteresis was observed in these samples. These results implied that all samples exhibited superparamagnetic behavior (Xing et al., 2023). This superparamagnetic behavior was advantageous for the convenient separation of Fe_3O_4@CS@RhDypB from the solution, especially when Fe_3O_4@CS@RhDypB was to be reused with the assistance of an external magnetic field.

3.3. *Optimization of preparation conditions for Fe_3O_4@CS@RhDypB*

To obtain the Fe_3O_4@CS@RhDypB with higher enzymatic activity recovery, the preparation conditions, such as the amount of enzyme, pH, temperature, the crosslinking time and the concentration of glutaraldehyde, were further optimized adopting a single-factor approach.

The effect of the amount of enzyme on the Fe_3O_4@CS@RhDypB was investigated (Fig. 4a). The maximum protein loading capacity of the magnetic chitosan carrier reached 30.78 mg/g when the amount of enzyme was 4 U (pH 6.0, 35 °C, crosslinking time 80 min and 2 % glutaraldehyde), indicating that the protein loading capacity reached saturation. However, when the amount of enzyme exceeded 3 U, there was a slight decrease in enzymatic activity recovery. This phenomenon may be attributed to overcrowding of space owing to an excess amount of enzyme. Therefore, to ensure full fixation of RhDypB on the carrier and to maintain high enzyme activity, the enzyme amount of 3 U was recommended.

More importantly, the immobilized pH and temperature would greatly affect the performance of Fe_3O_4@CS@RhDypB (Fig. 4b, c). The highest enzymatic activity recovery was observed at pH 6.0 (3 U enzyme, 35 °C, crosslinking time 80 min and 2 % glutaraldehyde) and 35 °C (3 U enzyme, pH 6.0, crosslinking time 80 min and 2 % glutaraldehyde). However, the enzymatic activity recovery declined as the pH and temperature deviated from these optimal values.

The crosslinking time was subsequently optimized (Fig. 4d). A short cross-linking time prevented enzyme molecules from fully contacting and binding to the carrier, resulting in a low enzyme activity recovery. Conversely, an excessively long cross-linking time resulted in an excessive amount of enzyme on the carrier, creating structural barriers for the binding sites of enzyme molecules and substrates. The maximum recovery of enzyme activity reached 55.21 % at the cross-linking time of 80 min (3 U enzyme, pH 6.0, 35 °C and 2 % glutaraldehyde).

The effect of different concentrations of glutaraldehyde on the enzymatic activity recovery was studied (Fig. 4e). The aldehyde group of glutaraldehyde underwent aldehyde amine condensation with chitosan or the amino group in the enzyme, which led to enzyme immobilization on the surface of magnetic chitosan. However, excessive concentration of glutaraldehyde could cause enzyme denaturation due to its organic nature. The highest enzymatic activity recovery was achieved when the glutaraldehyde concentration was 2 %. Based on the above data, the maximum enzymatic activity recovery was 55.21 % and the protein loading capacity was 24.60 mg/g under optimal immobilization conditions (3 U enzyme, pH 6.0, 35 °C, crosslinking time 80 min and 2 % glutaraldehyde). The enzymatic activity of Fe_3O_4@CS@RhDypB was

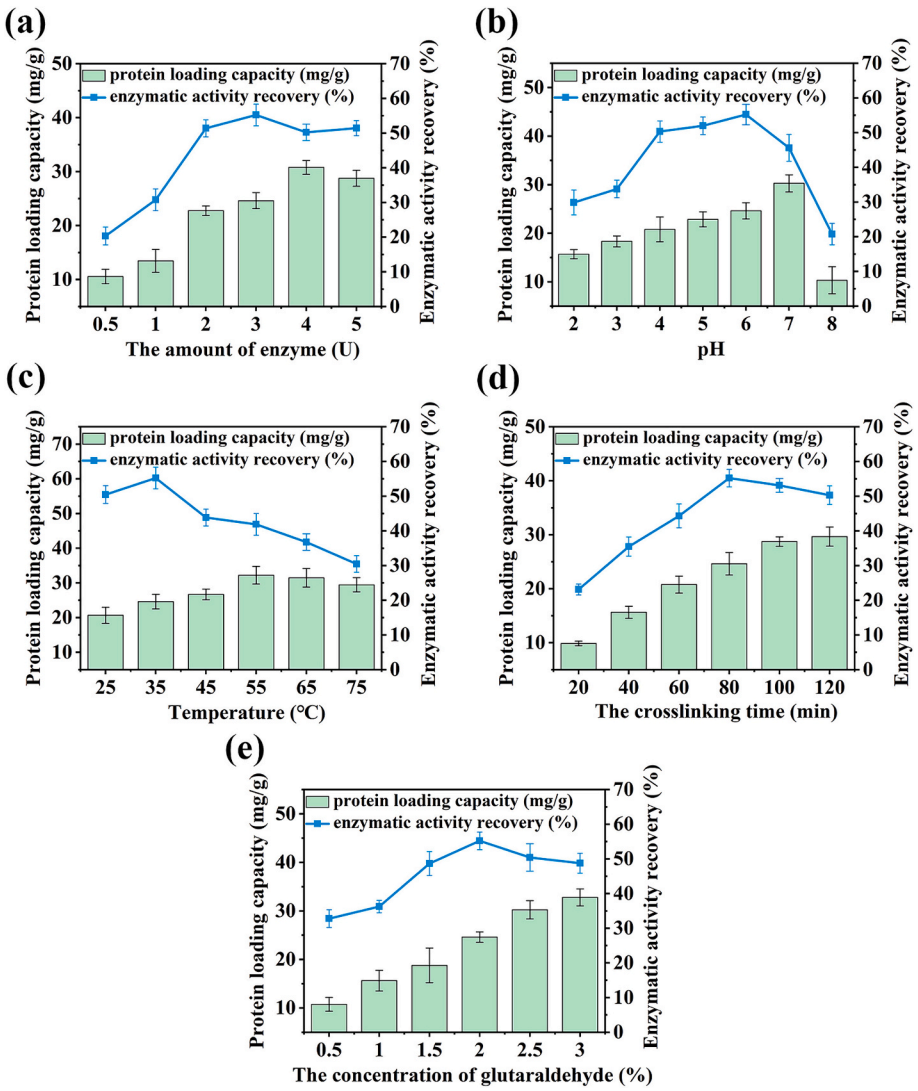

Fig. 4. Effects of different preparation conditions on the protein loading capacity and the enzymatic activity recovery of Fe_3O_4@CS@RhDypB. (a) The amount of enzyme. (b) pH. (c) Temperature. (d) The crosslinking time. (e) The concentration of glutaraldehyde.

determined as 4.89 U/mg at pH 4.0 and 30 °C before the optimization. Under the optimal immobilization conditions, the enzymatic activity of Fe_3O_4@CS@RhDypB reached 7.52 U/mg, revealing a 1.5-fold increase in the specific activity compared to the unoptimized conditions.

3.4. Enzymatic activity between free RhDypB and Fe_3O_4@CS@RhDypB

To the best of our knowledge, pH and temperature are crucial factors influencing the biocatalytic activity of enzymes. The effects of pH and temperatures on the relative activities of free RhDypB and Fe_3O_4@CS@RhDypB were examined through the oxidation of ABTS. It was observed that both free RhDypB and Fe_3O_4@CS@RhDypB showed the highest enzymatic activity at pH 4.0 and 65 °C, simultaneously, while Fe_3O_4@CS@RhDypB manifested a broader pH and temperature range. Both free RhDypB and Fe_3O_4@CS@RhDypB preferred the acidic reaction environment, while Fe_3O_4@CS@RhDypB maintained over 90 % relative activity within the pH range of 3.0 to 6.0 and over 75 % relative activity at pH 2.0 and 7.0 (Fig. 5a). This phenomenon could be ascribed to the chelating effect between the enzyme molecules and the Fe_3O_4@CS nanoparticles, which promoted the rigidity of enzyme and protected against conformational changes in the microenvironment (Simon-Herrero et al., 2019).

The enzymatic activity of Fe_3O_4@CS@RhDypB exhibited a substantial increase compared to free RhDypB across all temperature ranges (Fig. 5b). Significantly, the relative enzymatic activity remained above 90 % within the range of 45–75 °C and over 80 % within the range of 37–75 °C, which meant that the temperature spectrum of Fe_3O_4@CS@RhDypB was significantly wider than that of free RhDypB. The increase in resistance to temperature may be due to the abundant functional groups on the surfaces of carriers, which prevented the Fe_3O_4@CS@RhDypB from drastic conformational changes during temperature changes (Chen, Lam, & Yeung, 2011).

To investigate the storage stability of Fe_3O_4@CS@RhDypB, it was stored in sodium acetate buffer at pH 4.0, and the relative enzymatic activity was measured at various times and compared with that of the free RhDypB. The results demonstrated a significant improvement in the stability of RhDypB following immobilization (Fig. 5c). After 9 days of storage, the relative enzymatic activity of the free enzyme was only 4.20 %, while the Fe_3O_4@CS@RhDypB still maintained a relative enzymatic activity of 30.21 % even after 15 days of storage. The immobilized enzyme may experience constraint in flexibility due to the binding interactions between the enzyme and the carrier, thus preventing the loss of enzymatic activity (Coscolín et al., 2018).

The reusability of Fe_3O_4@CS@RhDypB was investigated (Fig. 5d). After determining the enzymatic activity, Fe_3O_4@CS@RhDypB was separated using magnet and immediately introduced into fresh reaction

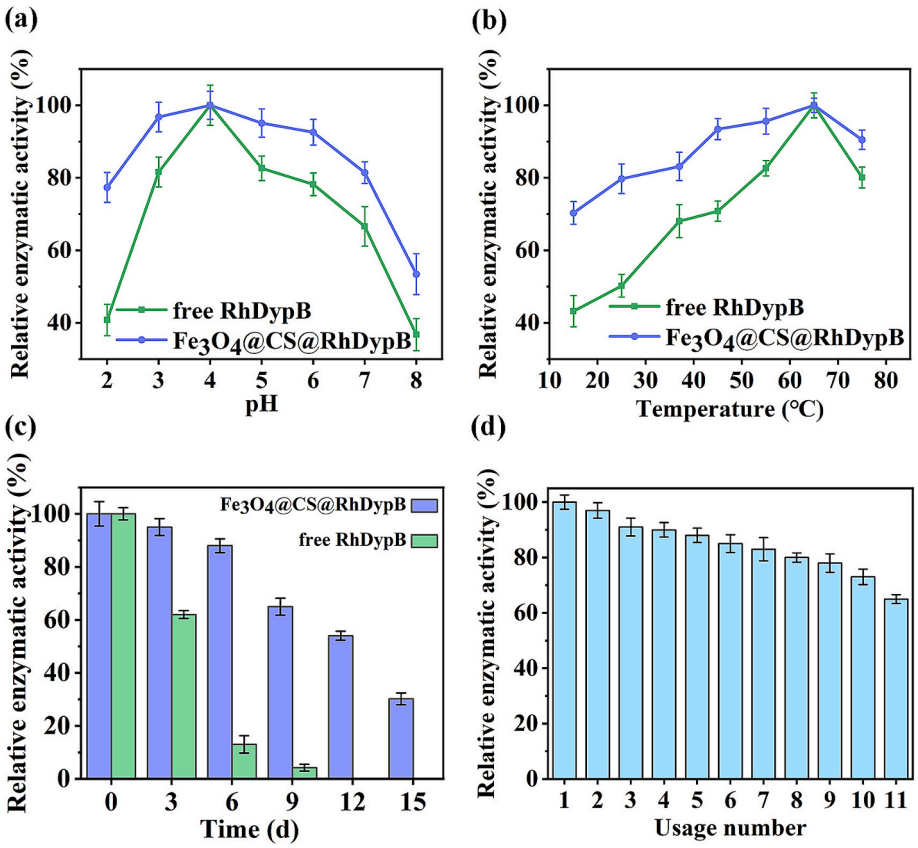

Fig. 5. Enzymatic activity between free RhDypB and Fe_3O_4@CS@RhDypB. (a) Effects of pH on the enzymatic activity of free RhDypB and Fe_3O_4@CS@RhDypB. (b) Effects of temperatures on the enzymatic activity of free RhDypB and Fe_3O_4@CS@RhDypB (c) Residual enzymatic activity of free RhDypB and Fe_3O_4@CS@RhDypB stored for various times. (d) Residual enzymatic activity of Fe_3O_4@CS@RhDypB after repeated utilization.

system for subsequent enzymatic activity assessment. The result showed that the Fe_3O_4@CS@RhDypB could retain 85.34 % of initial enzymatic activity after 6 rounds of usages, while 65.32 % of the initial enzymatic activity was retained after utilization for 11 times. These results indicated that Fe_3O_4@CS@RhDypB exhibited good reusability, compared with the free enzyme.

3.5. *Evaluation of mycotoxin degradation by Fe_3O_4@CS@RhDypB*

Due to the unique structural and catalytic properties of DyPs, they are capable of oxidizing a variety of phenolic compounds and other non-phenolic compounds, which are hardly subject to degradation (Colpa et al., 2014). Several earlier investigators have described that DyPs are involved in lignin degradation and industrial dye decolorization (Ahmad et al., 2011). However, limited studies reported that DyPs had degradation capability for mycotoxins. Herein, the common mycotoxins including AFB_1 and ZEN were used to evaluate the degradation ability of Fe_3O_4@CS@RhDypB. UPLC-TQD was used for qualitative and quantitative analysis of AFB_1 and ZEN, and standard curves were drawn according to the peak areas of AFB_1 and ZEN at different concentrations (Fig. S2). The concentrations of AFB_1 and ZEN were calculated according to the standard curve. The concentrations of AFB_1 and ZEN in the solution containing Fe_3O_4 or Fe_3O_4@CS were consistent with the control, which meant that the AFB_1 and ZEN were stable in the reaction matrix solution (Fig. 6a, b). In addition, the Fe_3O_4@CS@RhDypB was found to efficiently degrade two mycotoxins in the presence of Mn^{2+} and H_2O_2. In comparison, the mycotoxin contents in Fe_3O_4 or Fe_3O_4@CS decreased slightly after 24 h of treatment (Fig. 6c, d). The loss of mycotoxin contents may be attributed to the absorption of the carrier material. However, this effect of absorption was scarcely significant, corresponding to detoxification rates of 18.30 % and 15.56 % for AFB_1 and ZEN, respectively. While Fe_3O_4 and Fe_3O_4@CS exhibited some ability to degrade mycotoxins, this effect may be due to the absorption effect or the enzyme-like catalytic activity of the material, which slightly contributed to their overall efficacy (Gao et al., 2007). Despite the effect of the material, the mycotoxins were biologically degraded by the Fe_3O_4@CS@RhDypB, and the degradation rates of AFB_1 and ZEN were 85.61 % and 86.52 %, respectively, after 24 h reaction.

The BsDyP enzyme, derived from *Bacillus subtilis*, exhibits dye-decolorizing peroxidase activity. When employing APTS as a substrate, BsDyP demonstrated a significantly higher catalytic efficiency (k_{cat}/K_m = 35.7 $mmol^{-1}{\cdot}L{\cdot}s^{-1}$) compared to the RhDypB enzyme investigated in this study (Scocozza, Martins, & Murgida, 2021). It had been demonstrated that BsDyP was capable of efficiently degrading AFB_1 and ZEN with degradation rates of 76.93 % and 84.65 %, respectively, within 48 h (Qin et al., 2021). In comparison, our study achieved even higher degradation rates within a shorter timeframe. The most extensively studied enzyme for the biodegradation of ZEN is the zearalenone hydrolase ZHD101 from Clonostachys rosea, which can hydrolyze ZEN with a high degradation effect. However, the optimal reaction pH of ZHD101 was pH 10.5, which greatly limited its application in practical foodstuffs and environmental samples (Zhang, Xu, Wu, Zhang, & Mu, 2020). Fortunately, Fe_3O_4@CS@RhDypB was firstly found in this work that it can degrade ZEN at pH 4.0, providing another effective method for ZEN degradation. These results implied that Fe_3O_4@CS@RhDypB possessed efficient mycotoxin degradation capabilities and had potential applications in food and environment industry.

To have a preliminary glimpse if the mycotoxin was detoxified, it is essential to identify the degradation products of AFB_1 and ZEN. The main degradation products of AFB_1 and ZEN were analyzed by HPLC-MS (Fig. 6e, f). The parent ion appeared at m/z 329.064 $(M + H)^+$, while several diagnostic ions were observed at m/z 311.055 and m/z 283.059.

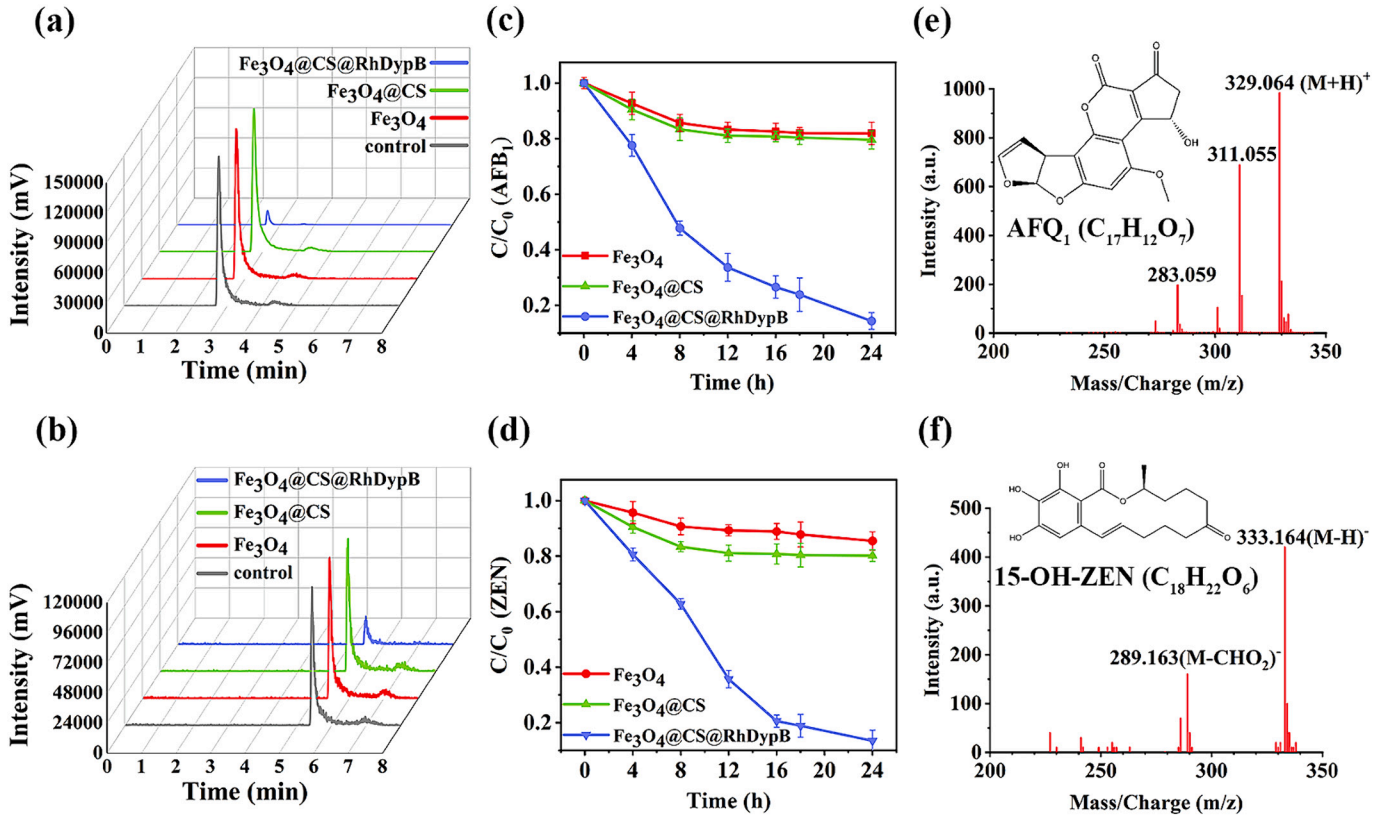

Fig. 6. Mycotoxin degradation analysis. (a) HPLC spectrogram of AFB_1 degradation. The red, green and blue lines represented the degradation of AFB_1 by Fe_3O_4, Fe_3O_4@CS, Fe_3O_4@CS@RhDypB respectively. The gray line represented blank control. (b) HPLC spectrogram of ZEN degradation. The red, green and blue lines represented the degradation of ZEN by Fe_3O_4, Fe_3O_4@CS, Fe_3O_4@CS@RhDypB respectively. The gray line represented blank control. (c) Detoxification effects of AFB_1 by Fe_3O_4, Fe_3O_4@CS, Fe_3O_4@CS@RhDypB. (d) Detoxification effects of ZEN by Fe_3O_4, Fe_3O_4@CS, Fe_3O_4@CS@RhDypB (e) The UPLC-MS analysis of AFB_1 degradation products. (f) The UPLC-MS analysis of ZEN degradation products. (For interpretation of the references to colour in this figure legend, the reader is referred to the web version of this article.)

These ions corresponded to the MS fragments of aflatoxin Q_1 (AFQ_1) (Loi et al., 2020), with a formula of $C_{17}H_{12}O_7$, suggesting that AFB_1 was hydroxylated to AFQ_1. Fortunately, AFQ_1 was found to exhibit significantly lower acute toxicity and mutagenicity compared to AFB_1 in rainbow trout (Loi et al., 2020). The degradation products of ZEN exhibited the parent ion at m/z 333.164 $(M\text{-}H)^-$ while generating a daughter ion of m/z 289.163 $(M\text{-}CHO2)^-$. These ions were consistent with the MS fragments of 15-OH-ZEN, with a formula of $C_{18}H_{22}O_6$. In addition, the estrogenicity of 15-OH-ZEN had been reported to be reduced by 98 % compared to ZEN (Qin, Su, et al., 2021). Previous studies had reported the degradation mechanism of DyPs on non-phenolic lignin via generating radicals with high redox potential (Catucci, Valetti, Sadeghi, & Gilardi, 2020). Similarly, the AFB_1 and ZEN degradation by RhDypB was achieved by the oxidation of free radicals. Overall, AFB_1 and ZEN were hydroxylated to AFQ_1 and 15-OH-ZEN, respectively, and the hydroxylation products were considered safe.

The reusability of immobilized enzyme was a critical parameter for its application in industry, as it directly impacted production costs (Zhang et al., 2020). As immobilized carriers, magnetic composite nanoparticles could separate immobilized enzymes from complex mixtures by an external magnetic field simply and efficiently (Cao et al., 2012; Liu et al., 2011). Therefore, it had great advantages over other immobilized carriers. In this work, the reusability of Fe_3O_4@CS@RhDypB was investigated by using AFB_1 and ZEN as enzymatic reaction

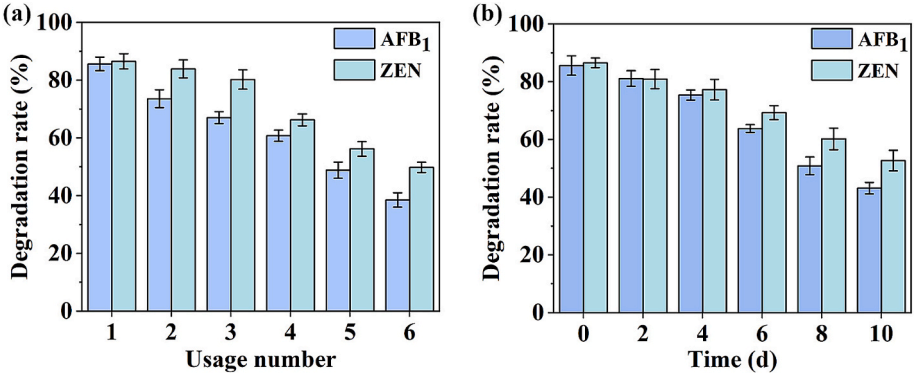

Fig. 7. The reusability and storage stability of Fe_3O_4@CS@RhDypB for mycotoxin degradation. (a) The reusability. (b) The storage stability.

substrates (Fig. 7a). The Fe_3O_4@CS@RhDypB was recycled using magnet after each mycotoxins degradation reaction for subsequent usage. In the first time of use, the degradation rates of AFB_1 and ZEN by immobilized RhDypB were 85.61 % and 86.52 %, respectively. Even after three times of applications, the Fe_3O_4@CS@RhDypB still retained about the 80 % degradation rate for ZEN. The degradation rates reached 38.50 % and 49.76 % for AFB_1 and ZEN after sixth round of use, respectively. The findings indicated that Fe_3O_4@CS@RhDypB could undergo up to five cycles of recycling for the degradation of mycotoxins. The loss of enzymatic activity with repeated use may be caused by the following factors, including enzyme loss from the carrier surface (Cui et al., 2015), inhibition of reaction products (Jordan, Kumar, & Theegala, 2011), and enzyme denaturation (Li et al., 2018).

In general, the free enzymes in solution were not stable during storage and lost their activity gradually (Simon-Herrero et al., 2019). To explore the storage stability of the Fe_3O_4@CS@RhDypB for mycotoxin degradation, the Fe_3O_4@CS@RhDypB was stored in 50 mmol/L malonate buffer (pH 4.0) at 4 °C up to 10 days, with daily testing of mycotoxin degradation (Fig. 7b). The results indicated that Fe_3O_4@CS@RhDypB degraded more than 70 % AFB_1 and ZEN after 5 days of storage. Furthermore, it can be seen that even after 10 days of storage, the Fe_3O_4@CS@RhDypB maintained degradation rates of 43.11 % and 52.67 % for AFB_1 and ZEN, respectively. The excellent storage stability was attributed to the chitosan layer on the surface of Fe_3O_4, which made RhDypB firmly immobilized on Fe_3O_4@CS and protected it from unfolding and denaturation (Simon-Herrero et al., 2019). These results indicated that Fe_3O_4@CS@RhDypB had excellent storage stability, which was an essential factor for ensuring its shelf life in the industrial field.

4. Conclusion

In this work, a new application of the dye-decolorizing peroxidase RhDypB was fulfilled by immobilization of the enzyme on magnetic nanoparticles for highly efficient simultaneous degradation of AFB_1 and ZEN. The resulting immobilized enzyme Fe_3O_4@CS@RhDypB, which can be conveniently separated using an external magnetic field, had been optimized for various immobilization parameters and its properties thoroughly characterized. Compared to the free enzyme, the immobilized form demonstrated a broader operational temperature and pH range. Impressively, the immobilized enzyme achieved high catalytic degradation ability to AFB_1 and ZEN, resulting in degradation rates of 85.61 % and 86.52 %. The degradation products were identified as AFQ_1 and 15-OH-ZEN with lower toxicity. Furthermore, it not only retained its efficient degradation ability after five successive reapplications, but also showed remarkable stability over a 10-day storage period. These findings offered valuable theoretical insights for the potential industrial application of Fe_3O_4@CS@RhDypB in degrading mycotoxins in the food and environmental sectors.

CRediT authorship contribution statement

Xinling Du: Writing – original draft, Methodology, Data curation. **Mumin Zheng:** Investigation, Formal analysis. **Han Zhang:** Visualization. **Yangyu Qiu:** Methodology, Data curation. **Fuchun Ji:** Validation. **Zishen Nie:** Visualization. **Huidong Xu:** Software. **Xiaoxuan Li:** Visualization. **Shijia Wu:** Supervision. **Zhouping Wang:** Funding acquisition. **Fuguo Xing:** Supervision, Resources. **Yu Xia:** Writing – review & editing, Supervision, Resources, Project administration, Conceptualization.

Declaration of competing interest

The authors declare that they have no known competing financial interests or personal relationships that could have appeared to influence the work reported in this paper.

Data availability

Data will be made available on request.

Acknowledgments

This work was supported by the National Key Research and Development Program of China (2021YFE0101800), the S&T Support Program of Jiangsu Province (BE2022324), the College Students' Innovative Entrepreneurial Training Plan Program of Jiangnan University.

Appendix A. Supplementary data

Supplementary data to this article can be found online at https://doi.org/10.1016/j.foodchem.2024.141341.

References

Adebo, O. A., Molelekoa, T., Makhuvele, R., Adebiyi, J. A., Oyedeji, A. B., Gbashi, S., & Njobeh, P. B. (2020). A review on novel non-thermal food processing techniques for mycotoxin reduction. *International Journal of Food Science & Technology, 56*(1), 13–27. https://doi.org/10.1111/ijfs.14734

Ahmad, M., Roberts, J. N., Hardiman, E. M., Singh, R., Eltis, L. D., & Bugg, T. D. H. (2011). Identification of DypB from *Rhodococcus jostii* RHA1 as a lignin peroxidase. *Biochemistry, 50*(23), 5096–5107. https://doi.org/10.1021/bi101892z

Alshannaq, A., & Yu, J. H. (2017). Occurrence, toxicity, and analysis of major mycotoxins in food. *International Journal of Environmental Research and Public Health, 14*(6). https://doi.org/10.3390/ijerph14060632

Cao, M., Li, Z. H., Wang, J. L., Ge, W. P., Yue, T. L., Li, R. H., & Yu, W. W. (2012). Food related applications of magnetic iron oxide nanoparticles: Enzyme immobilization, protein purification, and food analysis. *Trends in Food Science & Technology, 27*(1), 47–56. https://doi.org/10.1016/j.tifs.2012.04.003

Catucci, G., Valetti, F., Sadeghi, S. J., & Gilardi, G. (2020). Biochemical features of dye-decolorizing peroxidases: Current impact on lignin degradation. *Biotechnology and Applied Biochemistry, 67*(5), 751–759. https://doi.org/10.1002/bab.2015

Chaplin, A. K., Wilson, M. T., & Worrall, J. A. R. (2017). Kinetic characterisation of a dye decolourising peroxidase from *Streptomyces lividans*: New insight into the mechanism of anthraquinone dye decolourisation. *Dalton Transactions, 46*(29), 9420–9429. https://doi.org/10.1039/c7dt01144j

Chen, X. Q., Lam, K. F., & Yeung, K. L. (2011). Selective removal of chromium from different aqueous systems using magnetic MCM-41 nanosorbents. *Chemical Engineering Journal, 172*(2–3), 728–734. https://doi.org/10.1016/j.cej.2011.06.042

Chen, Z., Wang, X., Chen, Y., Xue, Z., Guo, Q., Ma, Q., & Chen, H. (2018). Preparation and characterization of a novel nanocomposite with double enzymes immobilized on magnetic Fe_3O_4-chitosan-sodium tripolyphosphate. *Colloids and Surfaces. B, Biointerfaces, 169*, 280–288. https://doi.org/10.1016/j.colsurfb.2018.04.066

Colpa, D. I., Fraaije, M. W., & van Bloois, E. (2014). DyP-type peroxidases: A promising and versatile class of enzymes. *Journal of Industrial Microbiology & Biotechnology, 41*(1), 1–7. https://doi.org/10.1007/s10295-013-1371-6

Coscolín, C., Beloqui, A., Martínez-Martínez, M., Bargiela, R., Santiago, G., Blanco, R. M., & Ferrer, M. (2018). Controlled manipulation of enzyme specificity through immobilization-induced flexibility constraints. *Applied Catalysis A: General, 565*, 59–67. https://doi.org/10.1016/j.apcata.2018.08.003

Cui, R., Bai, C. H., Jiang, Y. C., Hu, M. C., Li, S. N., & Zhai, Q. G. (2015). Well-defined bioarchitecture for immobilization of chloroperoxidase on magnetic nanoparticles and its application in dye decolorization. *Chemical Engineering Journal, 259*, 640–646. https://doi.org/10.1016/j.cej.2014.08.074

Engin, A. B., & Engin, A. (2019). DNA damage checkpoint response to aflatoxin B_1. *Environmental Toxicology and Pharmacology, 65*, 90–96. https://doi.org/10.1016/j.etap.2018.12.006

Escrivá, L., Font, G., Manyes, L., & Berrada, H. (2017). Studies on the presence of mycotoxins in biological samples: An overview. *Toxins, 9*(8). https://doi.org/10.3390/toxins9080251

Farimani, M. H. R., Shahtahmasebi, N., Rezaee Roknabadi, M., Ghows, N., & Kazemi, A. (2013). Study of structural and magnetic properties of superparamagnetic Fe_3O_4/SiO_2 core–shell nanocomposites synthesized with hydrophilic citrate-modified Fe_3O_4 seeds via a sol–gel approach. *Physica E: Low-dimensional Systems and Nanostructures, 53*, 207–216. https://doi.org/10.1016/j.physe.2013.04.032

Gao, L., Zhuang, J., Nie, L., Zhang, J., Zhang, Y., Gu, N., & Yan, X. (2007). Intrinsic peroxidase-like activity of ferromagnetic nanoparticles. *Nature Nanotechnology, 2*(9), 577–583. https://doi.org/10.1038/nnano.2007.260

Jordan, J., Kumar, C., & Theegala, C. (2011). Preparation and characterization of cellulase-bound magnetite nanoparticles. *Journal of Molecular Catalysis B: Enzymatic, 68*(2), 139–146. https://doi.org/10.1016/j.molcatb.2010.09.010

Li, R., Fu, G., Liu, C., McClements, D. J., Wan, Y., Wang, S., & Liu, T. (2018). Tannase immobilisation by amino-functionalised magnetic Fe_3O_4-chitosan nanoparticles and its application in tea infusion. *International Journal of Biological Macromolecules, 114*, 1134–1143. https://doi.org/10.1016/j.ijbiomac.2018.03.077

Lin, L., Wang, X. P., Cao, L. F., & Xu, M. Y. (2019). Lignin catabolic pathways reveal unique characteristics of dye-decolorizing peroxidases in *Pseudomonas putida*.

Environmental Microbiology, 21(5), 1847–1863. https://doi.org/10.1111/1462-2920.14593

Liu, X., Lei, L., Li, Y. F., Zhu, H., Cui, Y. J., & Hu, H. Y. (2011). Preparation of carriers based on magnetic nanoparticles grafted polymer and immobilization for lipase. *Biochemical Engineering Journal, 56*(3), 142–149. https://doi.org/10.1016/j.bej.2011.05.013

Loi, M., Renaud, J. B., Rosini, E., Pollegioni, L., Vignali, E., Haidukowski, M., & Mulè, G. (2020). Enzymatic transformation of aflatoxin B_1 by Rh_DypB peroxidase and characterization of the reaction products. *Chemosphere, 250*. https://doi.org/10.1016/j.chemosphere.2020.126296

Mangini, V., Rosini, E., Caliandro, R., Mangiatordi, G. F., Delre, P., Sciancalepore, A. G., & Loi, M. (2024). DypB peroxidase for aflatoxin removal: New insights into the toxin degradation process. *Chemosphere, 349*, Article 140826. https://doi.org/10.1016/j.chemosphere.2023.140826

Pickova, D., Ostry, V., Toman, J., & Malir, F. (2021). Aflatoxins: History, significant milestones, recent data on their toxicity and ways to mitigation. *Toxins, 13*(6). https://doi.org/10.3390/toxins13060399

Qin, X., Su, X., Tu, T., Zhang, J., Wang, X., Wang, Y., & Huang, H. (2021). Enzymatic degradation of multiple major mycotoxins by dye-decolorizing peroxidase from *Bacillus subtilis*. *Toxins (Basel), 13*(6). https://doi.org/10.3390/toxins13060429

Qin, X., Xin, Y., Su, X., Wang, X., Wang, Y., Zhang, J., & Huang, H. (2021). Efficient degradation of Zearalenone by dye-decolorizing peroxidase from *Streptomyces thermocarboxydus* combining catalytic properties of manganese peroxidase and laccase. *Toxins, 13*(9). https://doi.org/10.3390/toxins13090602

Rahmanpour, R., & Bugg, T. D. H. (2015). Characterisation of Dyp-type peroxidases from *Pseudomonas fluorescens* Pf-5: Oxidation of Mn^{II} and polymeric lignin by Dyp1B. *Archives of Biochemistry and Biophysics, 574*, 93–98. https://doi.org/10.1016/j.abb.2014.12.022

Roberts, J. N., Singh, R., Grigg, J. C., Murphy, M. E. P., Bugg, T. D. H., & Eltis, L. D. (2011). Characterization of dye-decolorizing peroxidases from *Rhodococcus jostii* RHA1. *Biochemistry, 50*(23), 5108–5119. https://doi.org/10.1021/bi200427h

Scocozza, M. F., Martins, L. O., & Murgida, D. H. (2021). Direct electrochemical generation of catalytically competent Oxyferryl species of classes I and P dye decolorizing peroxidases. *International Journal of Molecular Sciences, 22*(22). https://doi.org/10.3390/ijms222212532

Shi, Y., Ouyang, B. B., Zhang, Y. L., Zhang, W. L., Xu, W., & Mu, W. M. (2023). Recent developments of mycotoxin-degrading enzymes: Identification, preparation and application. *Critical Reviews in Food Science and Nutrition*, 1–16. https://doi.org/10.1080/10408398.2023.2220402

Simon-Herrero, C., Naghdi, M., Taheran, M., Kaur Brar, S., Romero, A., Valverde, J. L., & Sanchez-Silva, L. (2019). Immobilized laccase on polyimide aerogels for removal of carbamazepine. *Journal of Hazardous Materials, 376*, 83–90. https://doi.org/10.1016/j.jhazmat.2019.05.032

Sobral, M. M. C., Faria, M. A., Cunha, S. C., & Ferreira, I. M. P. L. V. O. (2018). Toxicological interactions between mycotoxins from ubiquitous fungi: Impact on hepatic and intestinal human epithelial cells. *Chemosphere, 202*, 538–548. https://doi.org/10.1016/j.chemosphere.2018.03.122

Sugano, Y., Muramatsu, R., Ichiyanagi, A., Sato, T., & Shoda, M. (2007). DyP, a unique dye-decolorizing peroxidase, represents a novel heme peroxidase family: ASP171 replaces the distal histidine of classical peroxidases. *Journal of Biological Chemistry, 282*(50), 36652–36658. https://doi.org/10.1074/jbc.M706996200

Sugawara, K., Nishihashi, Y., Narioka, T., Yoshida, T., Morita, M., & Sugano, Y. (2017). Characterization of a novel DyP-type peroxidase from *Streptomyces avermitilis*. *Journal of Bioscience and Bioengineering, 123*(4), 425–430. https://doi.org/10.1016/j.jbiosc.2016.12.001

Vaghari, H., Jafarizadeh-Malmiri, H., Mohammadlou, M., Berenjian, A., Anarjan, N., Jafari, N., & Nasiri, S. (2016). Application of magnetic nanoparticles in smart enzyme immobilization. *Biotechnology Letters, 38*(2), 223–233. https://doi.org/10.1007/s10529-015-1977-z

Vignali, E., Tonin, F., Pollegioni, L., & Rosini, E. (2018). Characterization and use of a bacterial lignin peroxidase with an improved manganese-oxidative activity. *Applied Microbiology and Biotechnology, 102*(24), 10579–10588. https://doi.org/10.1007/s00253-018-9409-3

Wang, M. X., Zhang, F. Y., Xiang, L., Li, M. S., Lu, Z. H., Wu, P., & Zhang, G. M. (2024). Enhancing the activity of zearalenone lactone hydrolase toward the more toxic α-zearalanol via a single-point mutation. *Applied and Environmental Microbiology*, 90. https://doi.org/10.1128/aem.01818-23

Wang, Y. X., Chen, Y., Jiang, L., & Huang, H. (2022). Improvement of the enzymatic detoxification activity towards mycotoxins through structure-based engineering. *Biotechnology Advances*, 56. https://doi.org/10.1016/j.biotechadv.2022.107927

Xia, Y., He, R., Sun, Y., Zhou, H. Y., Gao, M. J., Hu, X. Y., & Wang, Z. P. (2022). Food-grade expression of manganese peroxidases in recombinant *Kluyveromyces lactis* and degradation of aflatoxin B_1 using fermentation supernatants. *Frontiers in Microbiology, 12*. https://doi.org/10.3389/fmicb.2021.821230

Xia, Y., Qiu, Y., Wu, Z. F., Cheng, Q. Q., Hu, X. Y., Cui, X. B., & Wang, Z. P. (2022). Preparation of recombinant *Kluyveromyces lactis* agents for simultaneous degradation of two mycotoxins. *AMB Express, 12*(1), 20. https://doi.org/10.1186/s13568-022-01361-6

Xing, M. Y., Chen, Y., Dai, W. Q., He, X., Li, B. Q., & Tian, S. P. (2023). Immobilized short-chain dehydrogenase/reductase on Fe_3O_4 particles acts as a magnetically recoverable biocatalyst component in patulin bio-detoxification system. *Journal of Hazardous Materials, 448*. https://doi.org/10.1016/j.jhazmat.2023.130986

Xu, R., Bi, H. P., He, G. Y., Zhu, J. W., & Chen, H. Q. (2014). Synthesis of cu-Fe_3O_4@graphene composite: A magnetically separable and efficient catalyst for the reduction of 4-nitrophenol. *Materials Research Bulletin, 57*, 190–196. https://doi.org/10.1016/j.materresbull.2014.05.045

Zhang, K., Yang, W. Z., Liu, Y., Zhang, K. G., Chen, Y., & Yin, X. S. (2020). Laccase immobilized on chitosan-coated Fe_3O_4 nanoparticles as reusable biocatalyst for degradation of chlorophenol. *Journal of Molecular Structure, 1220*. https://doi.org/10.1016/j.molstruc.2020.128769

Zhang, Z., Xu, W., Wu, H., Zhang, W., & Mu, W. (2020). Identification of a potent enzyme for the detoxification of Zearalenone. *Journal of Agricultural and Food Chemistry, 68*(1), 376–383. https://doi.org/10.1021/acs.jafc.9b06223

Zhou, C., He, N. S., Lin, X. F., Liu, H. L., Lu, Z. H., & Zhang, G. M. (2024). Site-directed display of zearalenone lactonase on spilt-intein functionalized nanocarrier for green and efficient detoxification of zearalenone. *Food Chemistry*, 446. https://doi.org/10.1016/j.foodchem.2024.138804